Creatine transporter deficient rat show motor dysfunction linked with cerebellar alterations and muscle creatine deficiency without muscle atrophy

Lara Duran-Trio[1*], Gabriella Fernandes-Pires[1], Jocelyn Grosse[2], Ines Soro-Arnaiz[3], Clothilde Roux-Petronelli[1], Pierre-Alain Binz[1], Katrien De Bock[3], Cristina Cudalbu[4], Carmen Sandi[2] and Olivier Braissant[1]*

[1]Service of Clinical Chemistry, University of Lausanne and Lausanne University Hospital of Lausanne, Lausanne, Switzerland.

[2]Brain Mind Institute, Ecole Polytechnique Fédérale de Lausanne (EPFL), Lausanne, Switzerland.

[3]Department of Health Sciences and Technology, Swiss Federal Institute of Technology (ETH), Zurich, Switzerland.

[4]Centre d'Imagerie Biomedicale (CIBM), Ecole Polytechnique Fédérale de Lausanne (EPFL), Lausanne, Switzerland.
*Co-corresponding authorship

ABSTRACT

Creatine (Cr) is a nitrogenous organic acid and plays roles as fast phosphate energy buffer to replenish ATP, osmolyte, antioxidant, neuromodulator, and as a compound with anabolic and ergogenic properties in muscle. Cr is taken from the diet or endogenously synthetized by the enzymes AGAT and GAMT, and specifically taken up by the transporter SLC6A8. Loss-of-function mutations in the genes encoding for the enzymes or the transporter cause Cerebral Creatine Deficiency Syndromes (CCDS). CCDS are characterized by brain Cr deficiency, intellectual disability with severe speech delay, behavioral troubles, epilepsy and motor dysfunction. Among CCDS, the X-linked Cr transporter deficiency (CTD) is the most prevalent with no efficient treatment so far. Different animal models of CTD show reduced brain Cr levels, cognitive deficiencies and together they cover other traits similar to those of patients. However, motor function was poorly explored in CTD models and some controversies in the phenotype exist in comparison with CTD patients. Our recently described *Slc6a8*^{Y389C} knock-in (KI) rat model of CTD showed mild impaired motor function linked with morphological alterations in cerebellum, reduced muscular mass, Cr deficiency and increased guanidinoacetate content in muscle, although no consistent signs of muscle atrophy. Our results indicate that such motor dysfunction is due to both nervous and muscle dysfunction, suggesting that muscle strength and performance as well as neuronal connectivity might be affected by this Cr deficiency in muscle and brain.

INTRODUCTION

Creatine (Cr) is an organic compound used as fast phosphate energy buffer to replenish ATP by the Cr / phosphocreatine (PCr) / creatine kinase (CK) system, important in tissues with high energy demand such as muscle or brain. Additionally, Cr also works as osmolyte, as antioxidant and mimics a neuromodulator [1,2] .

Cr is taken from the diet or endogenously synthetized in a two-step pathway by the enzymes AGAT (arginine-glycine amidinotransferase) and GAMT (guanidinoacetate methyltransferase), and specifically transported into the cells by SLC6A8 (also called CRT, CreaT or CT1, henceforth CrT)[3]. Guanidinoacetate (GAA) is the intermediate product of the reaction and creatinine (Crn) is the spontaneous breakdown product of Cr.

Deficits in the endogenous synthesis or transport of Cr cause Cerebral Creatine Deficiency Syndromes (CCDS) [4-7]. CCDS are characterized by brain Cr deficiency, intellectual disability with severe speech delay and behavioral abnormalities. Seizures and motor dysfunction are more specifically found in GAMT and Cr transporter (CTD) deficiencies. Among CCDS, CTD is the more frequent one, with an estimated prevalence of about 2% of males with intellectual disability and, unlike the other two CCDS, with no efficient treatment so far [8]. CTD is an X-linked gene disorder caused by loss-of-function mutations in the *SLC6A8* gene.

Several animal models of CTD have been generated with ubiquitous deletions [9-11] or with a ubiquitous point mutation [12] in the *Slc6a8* gene. Other conditional, ubiquitous tamoxifen-induced [13] or brain-specific [14-18] knock-out (KO) mice for CrT were also developed to better understand the role of CrT in different contexts providing additional cues about CTD pathology.

Mouse and rat models of CTD with ubiquitous *Slc6a8* gene modification exhibit characteristics similar to those of CTD patients such as brain Cr deficiency, decreased body weight and cognitive deficits. In a complementary way, they cover together other features present in CTD patients such as the characteristic increase in urinary Cr/Crn ratio and behavioral abnormalities including autistic-like traits or seizures [9-12,14,16,19,20]. However, despite the effects of Cr in neuron morpho-functional development [21-23] and the well-known ergogenic and anabolic properties in muscle [24], motor function was poorly studied in CTD pathology. Only one CTD mouse model described a motor dysfunction phenotype and it was linked with Cr deficiency and impaired metabolism in muscle [11], although no Cr deficiency was found in muscle from the unique CTD patient analyzed for this [25].

Here we aim to shed some light on this controversy and explore motor function in the sole rat model of CTD recently described, *Slc6a8*^{Y389C} [12], taking advantage of the higher proximity of rats over mice to human physiology, biochemistry and behavior [26].

METHODS

Animals

Adult wild-type (WT) and knock-in (KI) *Slc6a8*$^{xY389C/y}$ males of 3-4 months of age were used for all the experiments; animals were genotyped and housed as previously described [12]. Rats were fed with a vegetarian diet devoid of Cr (Safe 150). All experiments were performed with the approval of the veterinary authorities of the Canton de Vaud (Switzerland; authorization VD-3284) and in accordance with the regulations of the Swiss Academy of Medical Science, as well as followed the ARRIVE Guidelines 2.0. Efforts were made to minimize stress and number of animals used.

Tissue collection

Animals were anesthetized with 4-5% isoflurane, plasma and urine were collected as previously described [12], then animals were sacrificed by rapid decapitation and brain and quadriceps were rapidly dissected out and prepared for biochemical or histological analysis.

Tissues for biochemical analysis were directly frozen and stored at -80ºC. Tissues for histological analysis were fixed in 4% paraformaldehyde (PFA) in PBS overnight at 4ºC, then rinsed with PBS and sunk in 18% (muscle) or 30% (brain) sucrose before being embedded in Tissue-Tek (OCT 4583, for muscle) or gelatin/sucrose (7.5% gelatin, Sigma-Aldrich G2500, 15% sucrose in phosphate buffer 0.1M pH 7.2, for brain), frozen and stored at -80ºC.

Determination of creatine, guanidinoacetate, creatine kinase, creatinine and acetylcholine

Plasmatic and urinary creatinine (Crn) was measured as previously described [12]. Plasmatic creatine kinase (CK) was measured on a COBAS8000 automate (Roche, Switzerland).

For intramuscular measure of creatine (Cr) and guanidinoacetate (GAA), 3 replicates per animal were used. Powder of frozen muscle was homogenized in H_2O at 4º by sonication (10 seconds) and centrifuged (10000g, 5min, 4ºC). The supernatant was used to measure Cr and GAA by liquid chromatography-tandem mass spectrometry as described in [12,27].

Acetylcholine determination in muscle samples was performed according to instructions (Sigma-Aldrich MAK056), using 3 replicates per animal. Total choline is the sum of free choline and acetylcholine.

Quantitative PCR

Muscle tissue (20mg) was homogenized with a tissue homogenizer (Omni THq) in 500µl ice cold TRIzol (Thermo Fisher, 15596018), after addition of 200µl chloroform, the homogenate was spun down for 15min at 12000g. The clear phase was mixed with 70% ethanol and transferred into a mRNA extraction column (Thermo Fisher, 12183018A). Subsequently, mRNA was extracted according to the manufacturer's instruction. The purity and quantity of mRNA was assessed by spectrophotometry (Tecan, Spark). mRNA was reverse-transcribed using High-Capacity cDNA Reverse Transcription Kit (Thermo Fisher, 4368813). A SYBER Green-based master mix (Thermo Fisher, A25778) was applied for real-time qPCR analysis and primers that were used are listed in **Table 1**. To compensate for variations in mRNA input and efficiency of reverse-transcription, 2 housekeeping genes were used (*GAPDH* and *rRNA 18S*). The delta-delta C_T method was used to normalize the data.

Table1. Primers used for qPCR

Gene	Forward primer	Reverse primer
ATROGIN1	ACCGGCTACTGTGGAAGAGA	CCTTCCAGGAGAGAATGTGG
ITCH	CCACCCACCCCACGAAGACC	CTAGGGCCCGAGCCTCCAGA
GABARAPL1	CATCGTGGAGAAGGCTCCTA	ATACAGCTGGCCCATGGTAG
REDD1	TGGTGCCCACCTTTCAGTTG	GTCAGGGACTGGCTGTAACC
GAPDH	ATGACTCTACCCACGGCAAG	TGGGTTTCCCGTTGATGACC
18S	GCCGCTAGAGGTGAAATTCTT	GAAAACATTCTTGGCAAATGCTT

Western Blot

Muscle tissue (20mg) was homogenized with a tissue homogenizer (Omni THq) in ice cold buffer (1:15 w/v): [50 mM Tris–HCl pH 7.0, 270 mM sucrose, 5 mM EGTA, 1 mM EDTA, 1 mM sodium orthovanadate, 50 mM glycerophosphate, 5mM sodium pyrophosphate, 50 mM sodium fluoride, 1mM DTT, 0.1% Triton-X 100 and a complete protease inhibitor tablet (Roche Applied Science)]. Homogenates were centrifuged at 10000g for 10min at 4°C. Supernatant was collected and stored at -80°C for further analysis. Protein concentration was measured using the DC protein assay kit. 10µg of total protein was loaded in a 15-well pre-casted gradient gel (Bio-rad, 456-8086). After electrophoresis, a picture of the gel was taken under UV-light to determine protein loading using strain-free technology. Proteins were transferred via wet transfer on a PVDF membrane (Bio-rad, 170-4156) at 80 V for 90min and subsequently blocked for 1h at room temperature with 5% milk in TBS-Tween. Membranes were incubated overnight at 4°C with the following primary antibodies phospho-S6K1 Thr389 (pS6K1, Cell signaling, 9234); phospho-S6 Ribosomal Protein Ser235/236 (pRPS6, Cell signaling, 2211); S6K1 (Cell signaling, 9202); S6 Ribosomal Protein (RPS6, Cell signaling, 2217). The appropriate secondary antibodies for anti-rabbit IgG HRP-linked antibodies (Cell signaling, 7074) were used for chemiluminescent detection of proteins. Membranes were scanned with a chemidoc imaging system (Bio-rad) and quantified using Image lab software (Bio-rad).

Histology

Cryopreserved tissue was cut with a cryostat (Leica) at 20 µm thickness and slices were mounted over microscope slides, then warmed over a surface (~40ºC) for 20min, tempered, and frozen at -80ºC until use for immunofluorescence or for hematoxylin-eosin staining.

Immunofluorescence

For immunofluorescence, slides were tempered for 15min at room temperature (RT), incubated with 4% PFA in PBS for 30min at RT and washed 3 times with PBS for 5min each. Then slides were put in blocking solution (1% bovine serum albumin, Sigma-Aldrich A3912, in PBS) for at least 30min at RT before the overnight incubation at 4ºC with primary antibodies in blocking solution (1:100; anti-MAP2(A/B), MAB378; anti-pNF-M(NN18), MAB5254; anti-NF-M (RM044), MAB5254; anti-MBP(F6), sc-271524; anti-NeuN, MAB377; anti-GFAP, Abcam 7779-500; anti-Aqp4 (C-term), AB3594). Later, slides were washed three times for 5min each with PBS, incubated with secondary antibody (1:200; goat anti-rabbit-A555, A21429, or goat anti-mouse-A555, A21422) in blocking solution for 1h at RT, washed three times for 5min each with PBS, incubated with DAPI (Thermo Fisher D1306, 1:5000 in PBS) for 5min, washed with PBS for 3 times 5min each, and mounted with Anti-Fade Fluorescence Mounting Medium (ab104135).

For Bungarotoxin staining, slides were tempered for 15 min RT and processed according to instructions using α-Bungarotoxin CF-568 (biotium 0006).

Hematoxylin-eosin staining

For histological staining, slides were tempered for 15min RT and then immersed in distilled water, dehydrated with ethanol in increasing concentrations (25, 50, 75, 90, 95, 100% ethanol, 3min each), rehydrated with ethanol in decreasing concentrations (3min each from 100 to 25% ethanol) to distilled water, before doing the staining. For hematoxylin-eosin staining, slides were incubated 5min in Ehrlich Eosin (Fluka) at RT, washed with water, incubated 2min with Harris Hematoxylin (Histolab), washed

with water, dehydrated in increasing concentrations of ethanol till 100%, incubated in xylol for 3min, mounted in Eukitt (Biosystems) and let dry 24h at RT.

Golgi-Cox staining

For Golgi-Cox staining, dissected fresh brain was cut coronally in 3 parts and processed according to instructions (FD Rapid GolgiStain kit, PK401). PolyFreeze tissue freezing medium (Polysciences 19636-1) was used to cryopreserve the pieces. Cerebellum was cut sagittally at 300 µm thickness with a cryostat (Leica) and processed according to instructions.

Imaging and quantifications

Images of histochemical staining from muscle were taken using an OLYMPUS microscope, cross-sectional areas and minimum Feret diameter were obtained with ImageJ. Fluorescence images were taken using a ZEISS Axioscan Z1 and a confocal LSM780 microscope (ZEN software). Parameters of acquisition were optimized at the beginning of the experiment for each antibody (including conjugated CF-568 α-Bungarotoxin) and held constant. Maximal intensity z-projection of neuromuscular junctions (α-Bungarotoxin staining) was used for the blind analysis of the area, perimeter and intensity of the staining using ImageJ. Maximal intensity z-projection was done with the same number of slides (same z-thickness) for brain. Thickness from granular and molecular layers of cerebellum was measured using ImageJ along one comparable cerebellum slice per animal, then the average value from each animal was used for the analysis between genotypes. Images of dendritic spines were taken from terminal dendrites of Purkinje neurons using an OLYMPUS microscope. Number of spines per length, spine head diameter and spine length were measured using ImageJ to evaluate spine density and spine morphology.

Behavioral tests

Locomotion, rearing supported and unsupported in an Open Field

Rats were introduced in a round (1m diameter) open arena with black walls and floor made of black PVC for 10min while spontaneous behavior was recorded with a videocamera. Average velocity, total distance moved and the time spent moving and not moving (considering the thresholds of 2 cm/s and 1.75 cm/s, respectively) were calculated using EthoVision tracking software. Rearing supported (standing on the hind limbs and one or two superior extremities) and unsupported (no superior limbs used) was hand-scored blindly with the Observer XT software, and cumulative duration, average duration per episode, latency to the first episode and frequency of such behaviors were analyzed.

Circular Corridor

Rats were individually placed for 30min in a black acrylic circular corridor with external and internal diameters of 50 and 40 cm, respectively, and a height of 40 cm. Average velocity, total distance moved and the time spent moving and not moving (considering the thresholds of 2 cm/s and 1.75 cm/s, respectively) were calculated using EthoVision tracking software.

Statistical analysis and graphs

All statistical analysis and graphs were conducted with R-3.5.1 [28]. A Shapiro test was used to assess the normality of each sample. To address the significance between WT and KI groups, Mann-Whitney tests were performed when normality was rejected while, for normal distributions, we used Bartlett tests to evaluate equality of variances and t-tests for equality of the means. 2-way ANOVA was used for the analyses of gene expression and mTOR readouts, and significant p-values from Tukey post hoc analysis are reported in the figures. Generalized linear mixed models blocking litter as random factor were used for the analysis of behavioral tests (package lme4 [29]), and the obtained coefficients (mean and standard

error of the mean) were used for the graphs. Graphs were done using ggplot2 package [30]. P-values are reported in figure legends, with the second decimal rounded to the nearest figure. Statistical significance was considered at the $P<0.05$ level.

RESULTS

Urinary and plasmatic Crn levels from *Slc6a8*$^{xY389C/y}$ KI males are strongly reduced

As previously shown [12], *Slc6a8*$^{xY389C/y}$ KI males exhibit the marker of CTD, an increased urinary Cr/Crn ratio. Such increase is due to a significant increase in urinary Cr concentration via CrT impairment in kidney cells and also to a strong significant reduction in urinary Crn levels (**Figure 1A** left panel). Given that Crn reuptake from the primary urine is negligible, we asked whether Crn levels in plasma were also decreased in KI males. As expected, plasmatic Crn levels in *Slc6a8*$^{xY389C/y}$ KI males were strongly and significantly reduced in comparison with those of WT males (**Figure 1A** middle panel) while plasmatic total creatine kinase (CK) only tended to decrease (**Figure 1A** right panel).

Muscle from *Slc6a8*$^{xY389C/y}$ KI males is Cr deficient and increases its GAA content

As mentioned before, Crn is the spontaneous breakdown product of Cr and muscle is the main storage of peripheral Cr. Therefore, low plasmatic and urinary levels of Crn indicate low concentration of Cr in muscle and/or low muscular mass [31]. We show here that Cr levels were significantly reduced in muscle from *Slc6a8*$^{xY389C/y}$ KI males (**Figure 1B** left panel). Interestingly, GAA could not be detected in muscle from WT males but it was significantly increased in that of *Slc6a8*$^{xY389C/y}$ KI males (**Figure 1B** right panel).

Slc6a8$^{xY389C/y}$ KI males exhibit reduced muscular mass and smaller myocytes

In order to evaluate muscular mass, we explored quadriceps muscle. Quadriceps from *Slc6a8*$^{xY389C/y}$ KI males were qualitatively thinner than those from WT males at 4 months of age (**Figure 1C**, note the rounded forms in WT in comparison with those of KI males), and this appearance was more pronounced with aging (data not shown). In addition, myocyte minimum Feret diameter and myocyte cross-sectional area from *Slc6a8*$^{xY389C/y}$ KI males were significantly reduced in comparison with those of WT males (**Figure 1D-E**). Neither vacuolization nor centralized nuclei were found in muscle from KI males.

Muscle from *Slc6a8*$^{xY389C/y}$ KI males show no sign of muscle atrophy

Reduced muscular mass and reduced myocyte size can be related to muscle atrophy [32], which was reported in two mouse models of CTD [11,33] despite no cases have been described in CTD patients as far as we know. We therefore wondered whether *Slc6a8*$^{xY389C/y}$ KI males present muscle atrophy.

Muscle atrophy occurs when the synthesis and degradation dynamic balance shifts towards protein degradation in response to a variety of stimuli, including infections, inflammation, oxidative and biomechanical stresses among others [32]. Such protein degradation is mainly mediated by the ubiquitin-proteasome system and autophagy via mTOR inhibition. FOXO-dependent genes, such as those encoding for E3 ubiquitin-ligases and autophagy-related proteins, are involved. Among these genes/proteins, we checked the gene expression of Atrogin-1 (an E3 considered a “master regulator” of muscle atrophy [34]), Itch/Aip4 (another E3 negatively regulating hypertrophy [35]), Gabarpl1/Gec1/Atg8l (implicated in autophagy [36]), as well as the levels of mTOR targeted proteins such as pS6K and pRPS6.

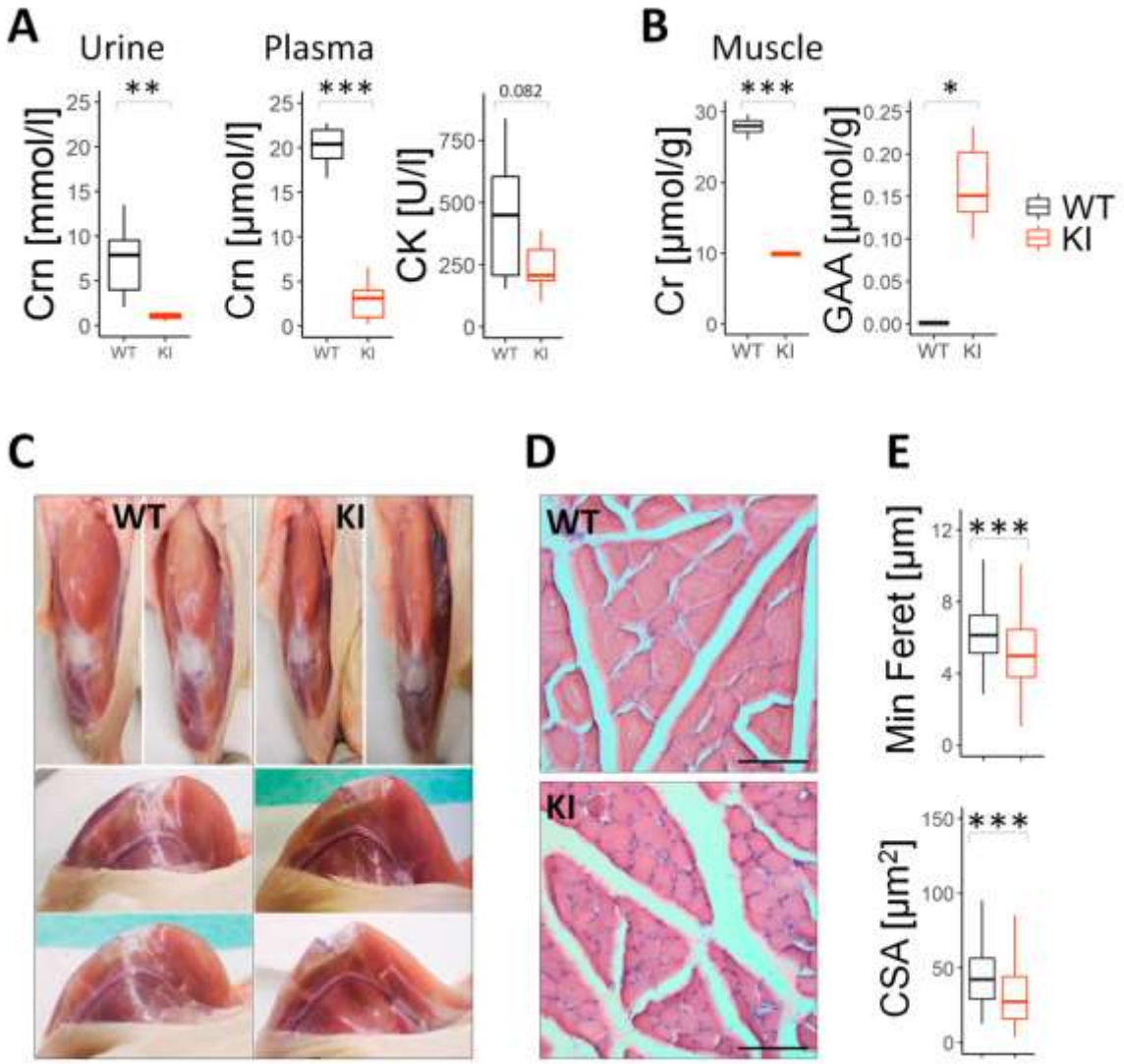

Figure 1: *Slc6a8*$^{xY389C/y}$ KI males present reduced muscular mass and smaller myocytes.

A: Urinary Crn levels (left panel) and plasmatic Crn and total CK levels (middle and right panel, respectively) as indicative of the muscular mass. 6WT and 6KI; two-tail t-test.

B: Significant decrease of Cr levels ([µmol/g tissue], two-tail t-test) and significant increase of GAA levels in muscle ([µmol/g tissue], Mann-Whitney test) in KI male rats. 5WT and 5KI.

C: Representative macroscopic pictures of WT and KI male hind limbs in frontal/ longitudinal (upper panel) and medial/inner lateral views (lower panels) showing reduced volume of quadriceps in KI male rats.

D: Representative microscopic pictures of hematoxylin/eosin staining in transversal sections of WT and KI male quadriceps showing significant smaller myocyte diameter in KI males. Scale bar=15µm.

E: Quantifications of myocyte minimum Feret diameter and cross-sectional area per each genotype. Mann-Whitney test, 3WT and 3KI (319-382 measurements per WT and 414-555 per KI male)

**P*<0.05, ***P*<0.01, ****P*<0.001. Statistical analysis was conducted with R-3.5.1 [28]. Graphs were done using ggplot2 package [30].

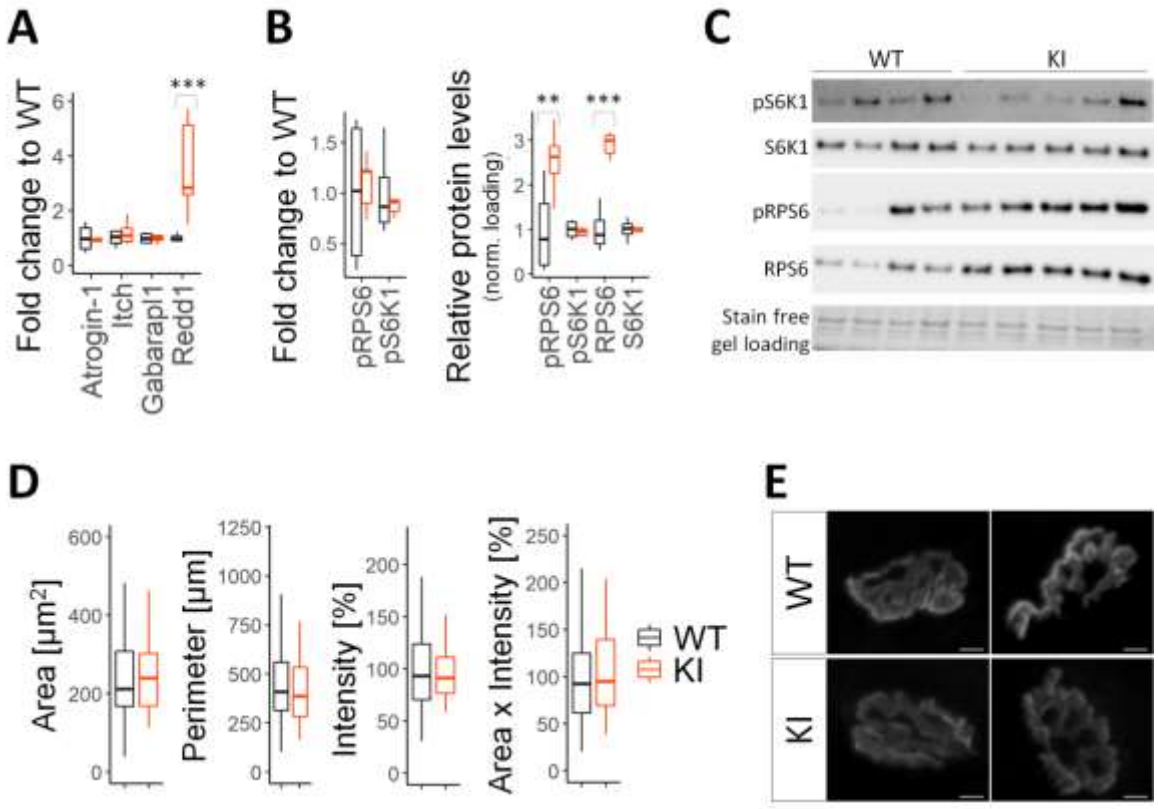

Figure 2: *Slc6a8*$^{xY389C/y}$ KI males do not show consistent signs of muscle atrophy.

A: Muscle expression levels (by quantitative PCR) of Atrogin-1, Itch and Gabarapl1 are similar between genotypes and that those of Redd1 significantly increased in muscle from KI males in comparison with those of WT males (orange and black boxes, respectively). 18S was used as housekeeping gene for normalization. 4 WT and 5 KI; 2-way ANOVA and Tukey posthoc test.

B: Relative levels of phosphorylated S6K1 (pS6K1) and RPS6 (pRPS6) over total S6K1 and RPS6, respectively, were similar between genotypes (left panel). Relative total and phosphorylated protein levels of RPS6 were significantly increased in muscle from KI males while those of S6K1 were similar between genotypes (right panel). 4 WT and 5 KI; 2-way ANOVA and Tukey posthoc test.

C: Representative western-blot from muscle of WT and KI males.

D: Boxplots showing no significant differences between genotypes in the area (in µm^2), perimeter (in µm), intensity (in % from WT mean value) or the combination of area and intensity (area multiplied by intensity, in % from WT mean value) of individual endplates stained with alpha-bungarotoxin from muscle of WT and KI males. 3 WT and 3 KI using around 35 pictures per animal; Mann-Whitney test.

E: Representative z-projection confocal images of individual endplates from WT and KI males using alpha-bungarotoxin staining. Scale bar is 5 µm.

***P*<0.01, ****P*<0.001. Statistical analysis was conducted with R-3.5.1 [28]. Graphs were done using ggplot2 package [30].

Interestingly, no significant differences were found between genotypes in the expression of atrogenes, ubiquitin-ligases or autophagy related genes (**Figure 2A and Supplementary Figure 1**, using two different housekeeping genes for normalization). In contrast, Redd1, a stress response gene also involved in mTOR inhibition [37], was significantly increased in muscle from KI males. Moreover, similar levels of the readouts of mTOR activation, the phosphorylated S6K1 (pS6K1) and RPS6 (pRPS6) over total S6K1 and RPS6, respectively, were found in muscle from both genotypes (**Figures 2B-C**). Intriguingly,

levels of total and phosphorylated ribosomal protein RPS6 (a substrate of S6K1 and other kinases [38]) but not those of S6K1 were significantly increased in muscle from KI males (**Figures 2B-C**).

On the other hand, motor endplate (the specialized postsynaptic region of a muscle cell) is reported to be structurally altered in cases of muscle atrophy such as sarcopenia [39]. We checked it by using the well-established bungarotoxin staining taking advantage of its binding to the nicotinic acetylcholine receptor at the postsynaptic muscle fibers. No apparent fragmentation of endplates was observed in muscle from any genotype, and area, perimeter and intensity of the staining were similar in muscle from both WT and KI males (**Figure 2D-E**).

Overall, these results show that muscle from *Slc6a8*$^{xY389C/y}$ KI males do not present signs of an atrophic process, although it seems that muscle cells are responding to some kind of stress.

Motor function is affected in *Slc6a8*$^{xY389C/y}$ KI males

Motor dysfunction is mentioned in 58% of CTD patients. The most prevalent symptom is hypotonia, while other observations are signs of spasticity, coordination dysfunction (such as unstable gait or clumsiness) and dystonia [40].

In order to assess motor function, we first checked signs of hypotonia by physical examination of the animals, then analyzed locomotion during free exploration (using the open field and circular corridor tests) as well as rearing, a typical spontaneous behavior requiring muscle performance as well as coordination and stability for its execution. Rearing can be described as standing up with hind limbs, being "supported" if one or both superior limbs are used or "unsupported" when no superior limbs are used.

Slc6a8$^{xY389C/y}$ KI males exhibited reduced body tension at around 4 months of age suggesting hypotonia, and frequent kyphosis or kyphoscoliosis worsening with aging (data not shown) suggesting muscle weakness. Additionally, in comparison with WT males, *Slc6a8*$^{xY389C/y}$ KI males showed a tendency to move less distance with less velocity in the open field test (**Figure 3A**) but moved significantly less distance, with significantly less velocity, and spent significantly less time moving in the circular corridor test (**Figure 3A**). A more detailed analysis along time showed that these differences between genotypes started from the minute 7 in the case of cumulative distance moved and average velocity, and from minute 1 for cumulative time moving in the circular corridor test, while no difference along time was found in the open field test (**Supplementary Figure 2**). Moreover, while *Slc6a8*$^{xY389C/y}$ KI males showed a significant decrease in unsupported rearing (**Figure 3B**, see the significant reduction in total duration, episode duration and frequency, and the tendency to increase latency), they did not show clear differences with WT males in supported rearing (**Figure 3C**). Furthermore, *Slc6a8*$^{xY389C/y}$ KI males appeared to be clumsy, being less dynamic and more instable (more tensed, sometimes vibrating) in equilibrium postures and falling down sporadically. All these results indicate altered motor function in *Slc6a8*$^{xY389C/y}$ KI males.

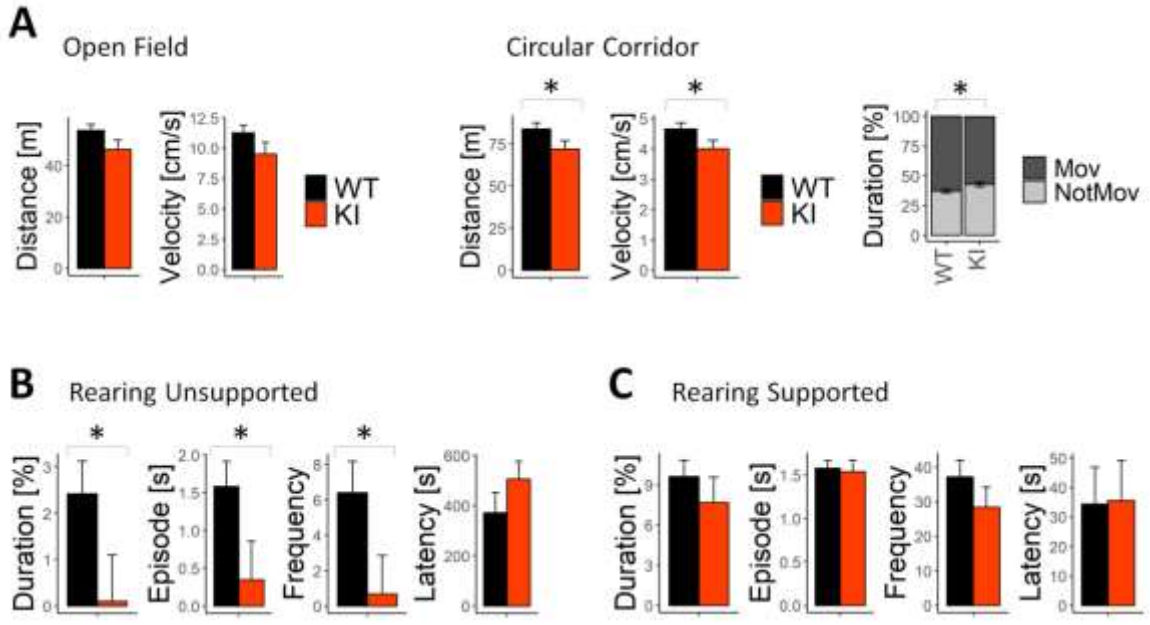

Figure 3: Motor function is affected in *Slc6a8*$^{xY389C/y}$ KI males at 3 mo.

A: In open field test, KI males (orange bars) tended to move less distance with less velocity in comparison with WT males (black bars); in circular corridor test, KI males moved significantly less distance with less velocity and spent significantly less time moving (Mov) than WT males (gray bars). 10 WT and 10 KI males.

B-C: KI males showed significant differences in unsupported (no superior limbs used, **B**) but not in supported (**C**) rearing. 9 WT and 10 KI males.

Linear mixed models blocking litter as random factor. **P*<0.05. Statistical analysis was conducted with R-3.5.1 [28], package lme4 [29]. Graphs were done using ggplot2 package [30].

Cerebellum from *Slc6a8*$^{xY389C/y}$ KI males is altered

Motor function depends on muscle and brain functions. One of the brain regions involved in motor function is cerebellum. Cerebellum presents very high levels of Cr in WT males and its Cr content is strongly decreased in *Slc6a8*$^{xY389C/y}$ KI males [12]. We thus analyzed whether cerebellum from *Slc6a8*$^{xY389C/y}$ KI males was affected by Cr deficiency using markers of brain cell types.

Immunostainings of MAP2(A/B), a protein associated with microtubules present in dendrites and soma of neurons [41], and NF-M/pNF-M, a neurofilament present mainly in soma of neurons when dephosphorylated or in axons when phosphorylated [22,42], showed a decreased staining in both granular and molecular layers of cerebellum from *Slc6a8*$^{xY389C/y}$ KI males (**Figure 4A**). However, no differences were shown in NeuN immunostaining (**Figure 4B**) where the number of NeuN-positive cells (neurons) did not change significantly between genotypes (data not shown).

Immunostaining of the myelin-basic protein (MBP) was patchy and decreased in *Slc6a8*$^{xY389C/y}$ KI males (**Figure 4A**). Immunostaining of Aqp4, a protein highly expressed at the blood-brain barrier present at the perimicrovessel astrocyte foot processes, glia limitans and ependymal [43], was similar among cerebellums from both genotypes (**Figure 4B**). Nevertheless, immunostaining of GFAP showed that astrocytes appeared increased in number in the granular layer (**Figure 4C** left panels) and that Bergmann glia processes were more tortuous in *Slc6a8*$^{xY389C/y}$ KI males (**Figure 4C** right panels). Moreover, despite the variability in the thickness of molecular and granular layers along cerebellum, the molecular but not the granular layer was significantly thinner in *Slc6a8*$^{xY389C/y}$ KI males (**Figure 4E**).

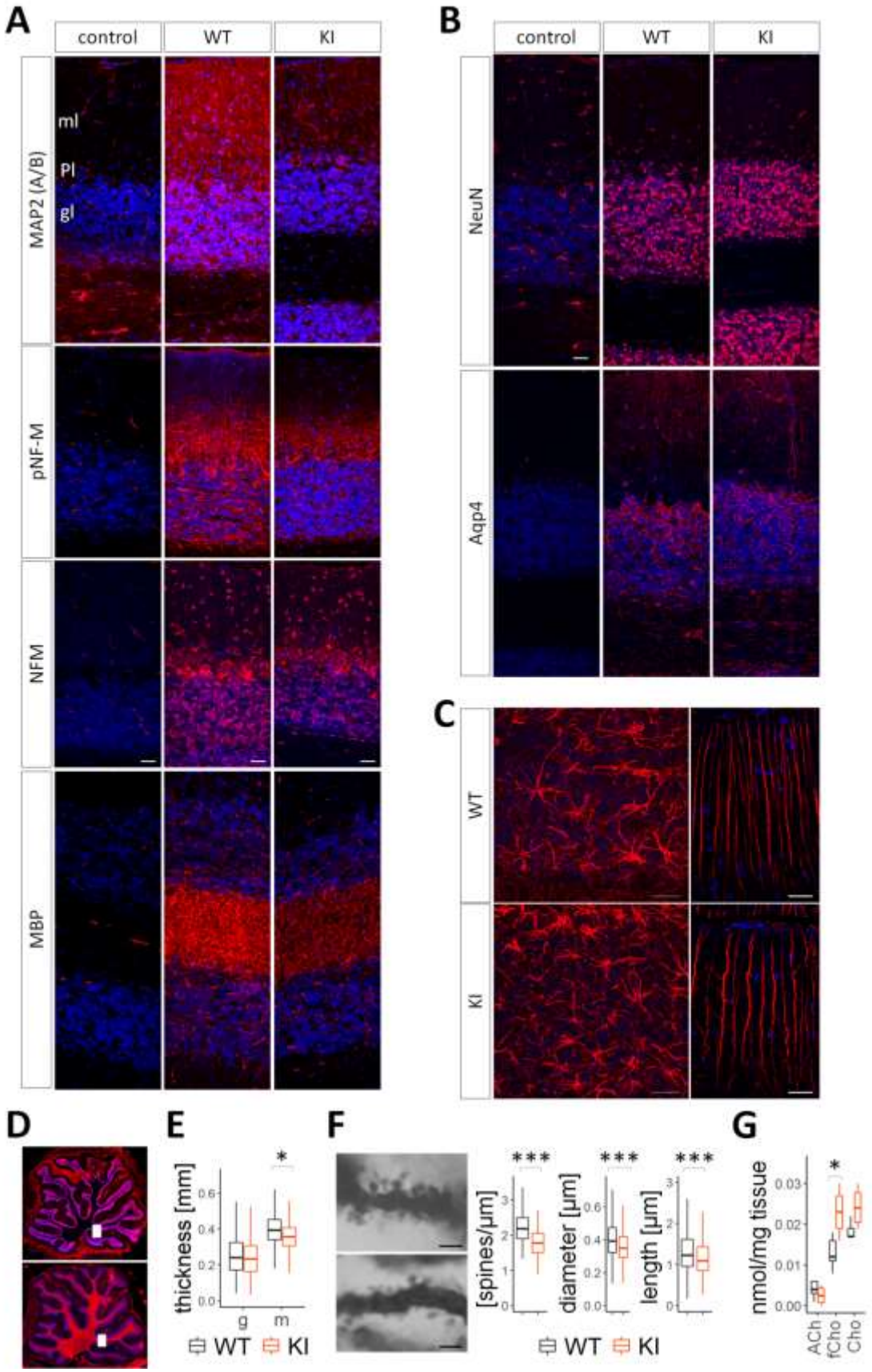

Figure 4: Cerebellum from *Slc6a8*$^{xY389C/y}$ KI males is affected at 3 mo.

A: Representative confocal z-projection images of MAP2 (A/B), pNF-M, NF-M and MBP immunostainings (in red, DAPI in blue) showing a decrease immunostaining in KI males.

B: Representative confocal z-projection images of NeuN and Aqp4 immunostainings showing no differences between WT and KI males.

C: Representative confocal images of GFAP immunostaining from granular layer (z-projection, left pictures) and molecular layer (slice of 0.30µm thickness, right pictures).

D: Epifluorescence pictures from cerebellum in sagittal sections showing with white squares the regions in which confocal images were taken. All images correspond to the region labeled in the top picture except the one for the MBP immunostaining (in A) which corresponds to the region labeled in the bottom picture.

E: Quantification of molecular and granular layers thickness showing a significant reduction in the molecular (m) but not the granular (g) layer of KI males. Mann-Whitney test, **P*<0.05, 4 WT and 4 KI (average values from each animal were used for the analysis between genotypes –details in methods' section--, plots showing the variability of all measurements).

F: Representative images of Purkinje terminal dendrites from WT and KI males (top and bottom panels, respectively), and quantifications of spine density (left, 101 and 72 measurements from WT and KI respectively), head diameter (middle, 2024 and 1322 spines from WT and KI respectively) and spine length (right plot, 2368 and 1491 spines from WT and KI respectively) showing a significant reduction of the three measurements in KI males. Mann-Whitney test, 4 WT and 3 KI (3-4 neurons per animal; 20-30 measurements per rat for spine density, 410-620 spines per rat for head diameter and spine length), ****P*<0.001.

G: Concentration of acetylcholine (Ach), free and total choline (fCho and Cho, respectively) in muscle from WT and KI males. 5 WT and 4 KI, t-test,**P*<0.05.

Calibration/scale bar in A, B and C represents 30µm; 2µm in F. Statistical analysis was conducted with R-3.5.1 [28]. Graphs were done using ggplot2 package [30].

In order to know whether these changes might have an impact in neuronal function, we analyzed dendritic spines of terminal dendrites from Purkinje neurons. Purkinje neurons are one of the largest neurons in the brain, being the sole output connection from cerebellar cortex and with an important role in motor coordination [44]. Spines are the postsynaptic compartment of excitatory synapses and their morphology correlates with synaptic strength, therefore changes in spine density and/or its morphology could reflect synaptic alterations affecting neuronal function [45]. Purkinje neurons from *Slc6a8*$^{xY389C/y}$ KI males showed significantly reduced spine density and spines significantly thinner and shorter than those from WT males (**Figure 4F**).

In summary, these results show that neurons, oligodendrocytes and astrocytes are affected in cerebellum from *Slc6a8*$^{xY389C/y}$ KI males, and together point towards altered morphology and connectivity which might have an impact in cerebellar function.

Acetylcholine levels do not change in motorneurons from KI males

Another important nervous actor involved in motor function is the motorneuron. Motorneurons innervates muscle via cholinergic neurotransmission in a specialized synapse called neuromuscular junction. Given the role of motorneurons in the pathology of certain muscular disorders [46], we wondered whether the neurotransmission from motorneurons to muscle was affected. To such aim, we evaluated the levels of the neurotransmitter acetylcholine (ACh) in muscle tissue, where the axonal terminals from motorneurons are present.

In muscle from KI males, acetylcholine levels did not change significantly although tended to decrease in comparison with those of WT males (-37%, **Figure 4G**). In contrast, levels of its precursor, free choline, were significantly increased (+77%, **Figure 4G**). This data reveals that final levels of the neurotransmitter tends to remain constant and that choline homeostasis is somehow affected in muscle of KI males.

DISCUSSION

We describe here the muscle and motor phenotype of the *Slc6a8*$^{xY389C/y}$ *in vivo* knock-in rat model of CTD. The brain Cr-deficient *Slc6a8*$^{xY389C/y}$ KI rat males are also muscle Cr-deficient and present less muscle bulk without signs of muscle atrophy, together with impaired motor function and morphological changes in cerebellum.

Reduced muscle bulk of *Slc6a8*$^{xY389C/y}$ KI males is supported by the significant low levels of plasmatic and urinary Crn (markers of low muscular mass [47]) and the presence of qualitatively thinner quadriceps. These results are in line with CTD patients, who frequently show reduced muscular mass [40] and decreased plasmatic Crn levels [8].

Apart of showing lower muscular mass, *Slc6a8*$^{xY389C/y}$ KI males also presented decreased muscle fiber size and lower muscle Cr concentration (-64%). Similar muscle phenotype was described in two CrT KO mouse lines [11,33] and was considered as "muscle atrophy". However, muscle atrophy is the process of muscle degradation/deterioration and such phenotype could be due to different causes, especially given the role of Cr in the development of muscle fibers [24] and as osmolyte contributing to the cellular volume [2]. One of these mouse lines showed a strong histological deterioration of muscle tissue in middle-age adults [33], but not at earlier ages, being a clear pathologic sign of an atrophic process. Nevertheless, this was not the case for the muscle from KI rat males, neither at older ages (e.g. 6 months-old, data not shown). Therefore, we performed more analyses in order to test whether the mentioned muscle phenotype was reflecting muscle atrophy. Interestingly, muscle from KI males did not show increases in the expression of genes involved in the atrophic process, nor changes in mTOR signaling or in the morphology of the endplates. These results indicate that such muscle phenotype is not related with muscle atrophy in KI rats. This may also be the case for the mentioned CrT KO mouse at earlier ages and for the other CrT KO mouse line [11] which showed reduced myocyte section area but no further histological alterations. Noteworthy, the contrast with that CrT KO mouse is not only in the severity of the muscle phenotype but also in life expectancy which is around 7 months of age in this mouse line while similar as WT in KI rats at least in the first year of life (no reports about life expectancy in the other CrT KO mouse lines are published). This difference might be due to the different impact of the mutations in the CrT or to the rodent mutant line background. Remarkably, such absence of atrophic process in muscle from KI males is in agreement with the absence of reported muscular atrophy in CTD patients, including the absence of structural alterations in muscle from the unique CTD patient deeply analyzed for this [25].

Reduced muscle bulk and smaller myocyte size in rodent models of CTD are in agreement. This reduction could be explained by the decreased Cr concentration in muscle, which has been observed in all the ubiquitous CTD rodent models [9-11] including the *Slc6a8*$^{xY389C/y}$ KI rat, and the roles of Cr in cellular volume and muscle development. Strikingly, no changes in cellular growth are suggested by the unaltered mTOR signaling, but we cannot discard modifications in other pathways related with muscle growth and differentiation. Nevertheless, although reduced muscle mass is a shared feature in patients and rodent models of CTD, myocyte size has not been analyzed yet in patients and the unique CTD patient analyzed exhibited normal muscle Cr levels [25]. However, it is possible that other muscles from the same patient were Cr deficient as it has been shown in vegetarians that muscle Cr concentration can

be reduced or similar to that of omnivorous people depending on the type of muscle being measured [48]. Additional studies will be needed to better characterize the muscle phenotype in CTD patients and to confirm whether muscle Cr levels do not change in human pathology, as well as to unravel the causes of such characteristic reduced muscular mass in conditions of CrT deficiency.

Noteworthy, two signals suggest that KI muscle cells are responding to some kind of stress: increased expression of Redd1 and increased levels of total and phosphorylated ribosomal protein RPS6. This correlates with Cr deficiency and might be induced by its direct or indirect consequences in cellular metabolism. Further investigations will be needed to disentangle the mechanisms involved in such response and whether there are potential therapeutic targets to prevent the muscle phenotype observed in CTD, to treat other pathological conditions and/or to use in the field of sports.

In the same line, we analyzed a qualitative marker of skeletal muscle microtrauma [47], plasmatic CK level. *Slc6a8*$^{xY389C/y}$ KI males showed low values but within a normal range, in line with the normal or decreased levels found in CTD patients [8]. This result do not support muscle damage, which is in agreement with the absence of centrally nucleated myofibers, but suggests that muscle CK content, and by extension muscle Cr content, might be reduced in *Slc6a8*$^{xY389C/y}$ KI males. Indeed, muscle Cr concentration was significantly decreased (-64%) in *Slc6a8*$^{xY389C/y}$ KI males.

Interestingly, this difference in muscle Cr concentration between the CTD patient and rodent models of CTD is paralleled to the plasmatic Cr level pattern, where patients show no significant changes in any and rodent models show a decrease in both [8,9,12]. Whether this difference is due to the diet (vegetarian diet used in some CTD models [11,12], while patients likely follow an omnivorous diet) in combination or not with intrinsic factors such as differential expression of Cr transporters among tissues and/or distinct regulation of biosynthesis and transport of Cr among species is still unknown.

Strikingly, this parallelism between Cr concentration in muscle and in plasma was observed not only in patients and animal models of CTD but in all CCDS, both in patients and animal models, where synthesis and/or transport of Cr is affected [8,9,12,49,50], as well as under Cr supplementation in conditions of low Cr levels and normal function of CrT in rodents and humans [48,50,51]. Therefore, although plasmatic Cr is not being used as marker of muscular mass, further studies might confirm it as marker of muscle Cr concentration, at least in circumstances of possible Cr depletion.

It is noteworthy that co-occurring with such a significant decrease in muscle Cr levels, muscle GAA concentration was significantly increased in *Slc6a8*$^{xY389C/y}$ KI males. Despite no available data from CTD patients, this result is similar to another CrT KO mouse [14]. Such increase in GAA content could indicate an attempt to compensate the Cr deficiency in rat muscle by increasing *de novo* synthesis of muscle Cr. Indeed, accumulation of AGAT was shown in muscle from a CrT KO mouse [11] and an increased in its expression was demonstrated in muscle from another CrT KO mouse [52] and in conditions of Cr depletion in kidney [53].

Together with this increase in muscle GAA levels, KI males also showed a significant augmentation in plasmatic GAA concentration [12]. Such double situation was also observed in patients and the mouse model of GAMT deficiency [8,49], suggesting that, similar to Cr, plasmatic GAA levels might inform about changes in muscle GAA concentration. Nevertheless, in contrast with Cr which both plasma and muscle levels are decreased in KI males around 3 times less than their respective WT values (**Table 2**), GAA levels increased by more than two orders of magnitude in muscle (x 126) and only twice in plasma from KI males. This pattern might reflect different regulation of Cr synthesis and/or GAA transport in different tissues (kidney-liver versus muscle). Moreover, by converting muscle GAA concentration from µmol per gram of tissue to µmol per ml (assuming that 70% of the tissue is water, **Table 2**), we were able to compare both muscle and plasmatic GAA levels in both genotypes. Intriguingly, while WT males showed that plasma had more GAA concentration than muscle, KI males presented the opposite pattern

having around one order of magnitude more concentration in muscle than in plasma. This dramatic change in GAA gradient between plasma and muscle might have consequences in the rest of the periphery. However, whether muscle is increasing the uptake together with the synthesis of GAA or whether it is providing GAA to the rest of the body (thus being as important as kidney) in conditions of CrT deficiency is not known.

Muscle Cr is also important for muscle strength and performance [54], and together with reduced muscle mass, reduced myocyte size and low muscle Cr content point towards low muscle performance likely affecting motor function.

Table 2: Comparison of metabolite concentrations (in µM = µmol/l) and their relative changes (%) in KI males with respect to those of WT males in urine, plasma and muscle. Average values (or median values if the distribution was not normal according to Shapiro test) per genotype of each metabolite concentration in urine, plasma and muscle. Concentration in muscle was transformed from µmol/g of tissue to µM assuming that tissue contains 70% of water. Part of the data was published in [12]. Significant differences between genotypes are recapitulated here and shown as *p<0.05, **p<0.01, ***p<0.001.

	Urine		Plasma		Muscle		Relative change (%)		
	WT	KI	WT	KI	WT	KI	urine	plasma	muscle
Crn	7340	950	20.15	2.65	NA	NA	12.9 **	13.2 ***	NA
GAA	620	1300	5	10	0.84	105.7	210.3	196.5 **	12583 *
Cr	280	9535	220	63	28000	10000	12109 **	32.2 ***	36.0 ***

Indeed, *Slc6a8*$^{xY389C/y}$ KI males exhibited signs of lower muscle tone (hypotonia) and muscle weakness in the early adulthood, and spent significantly less time moving from the first minute in the circular corridor test in comparison with WT males. Similar phenotype was found in a mouse model of CTD [11] and although muscle weakness is only rarely described in CTD patients, hypotonia is a frequent symptom [8]. This difference in the degree of severity is likely linked to the difference in muscle Cr concentration, namely higher muscle function impairment in conditions of Cr deficiency. Moreover, *Slc6a8*$^{xY389C/y}$ KI males showed other signs of motor dysfunction such as reduced locomotion and reduced unsupported rearing. The fact that *Slc6a8*$^{xY389C/y}$ KI males performed supported rearing similar as WT males and showed only a tendency to reduce locomotion in the open field test reveals that the phenotype of motor dysfunction is not too severe or disabling. In the circular corridor test, a better test than open field to evaluate locomotion in a spontaneous behavior, the differences in cumulative distance moved and average velocity appeared only with time. This effect seems to be more related with lower muscle endurance although we cannot discard dysfunctions from central nervous system. On the other hand, *Slc6a8*$^{xY389C/y}$ KI males accomplished supported but not unsupported rearing as WT males, revealing that *Slc6a8*$^{xY389C/y}$ KI males had problems with the extra level of difficulty involving stability, coordination and muscle strength. These symptoms of motor dysfunction are in line with those found in CTD patients [8,40] and with a CTD mouse model [11]. These impairments in motor function can be due to altered muscle and to altered central nervous system function. However, the contribution of each one to the motor dysfunction phenotype is not easy to detangle.

Alterations in CNS areas have been described in CTD patients [8] and in different mouse models of CTD [9,14,16]. However, cerebellum, a brain region with high Cr content involved in coordination and balance, and with abnormalities in CTD patients, has been very little explored so far. We have previously shown

that cerebellum from KI males exhibits a strong Cr deficiency [12]. We analyzed here its morphology and markers of different cell types by immunofluorescence. Similar number of NeuN-positive cells but changes in the staining of proteins related with neuronal cytoskeleton such as MAP2(A/B) and NF-M point that the number of neurons did not change although both dendritic trees and axons might be altered in cerebellum from *Slc6a8*$^{xY389C/y}$ KI males. This together with the decreased MBP staining, which is in agreement with the delayed myelination seen in some CTD patients [8], suggests that neuronal connectivity might be affected in this conditions of Cr deficiency [21,22].

Interestingly, differences in the pattern of GFAP staining both in granular and molecular layers indicates that astrocytes are disturbed in *Slc6a8*$^{xY389C/y}$ KI males although they are not a direct targeted cell in CTD since they do not usually express CrT [55]. Bergmann glia has a role in early development of the cerebellum assisting the migration of granule cells to the internal granular layer [56]. It is also required for synaptic pruning and it is intimately associated with Purkinje cells [57,58]. Given the reduced thickness of molecular layer and the tortuous processes of Bergmann glia in *Slc6a8*$^{xY389C/y}$ KI males it might be possible that the migration of the cells was altered and that Purkinje cells were affected as well. In fact, the shorter thickness of molecular layer and the reduced labeled in MAP2 suggest that dendritic tree of Purkinje cells is reduced. In order to see whether these morphological alterations have an impact in neuronal function, we analyzed the dendritic spines from Purkinje neurons, the sole output from cerebellar cortex. Morphology of these excitatory postsynaptic compartments correlates with synaptic strength and could indicate modifications in neuronal function [45]. Strikingly, Purkinje neurons from *Slc6a8*$^{xY389C/y}$ KI males showed significant less spine density and spines significantly shorter and thinner than those from WT males. This pattern indicates that Purkinje neurons might present less excitatory inputs and lower synaptic strength resulting in a decreased signaling [59], which could alter cerebellar function and in turn lead to motor dysfunction. These limitations in the number and size of dendritic spines could be due to either modifications in the neuronal network triggering changes in connectivity and/or to intrinsic structural and metabolic alterations linked to Cr deficiency, likely including a more or less compromised energy state of the cell.

We show for the first time alterations in cerebellum from an animal model of CTD. We previously demonstrated that cerebellum from *Slc6a8*$^{xY389C/y}$ KI males is Cr deficient [12] and here we present morphological changes which are in line with the abnormalities seen in CTD patients [8]. Neurons, astrocytes and oligodendrocytes are affected by such Cr deficiency in cerebellum from *Slc6a8*$^{xY389C/y}$ KI males. Noteworthy, we demonstrate that *in vivo* Cr deficiency causes alterations in spine density and spine morphology in Purkinje cells, limiting the number of spines and their size. Finally, all these morphological changes in cerebellum could have an impact in cerebellar function contributing to the motor dysfunction phenotype of *Slc6a8*$^{xY389C/y}$ KI males.

Moreover, we also explored whether motorneurons were involved in this motor function impairment. Levels of the neurotransmitter acetylcholine remained constant although tended to decrease in motorneurons from KI males, as acetylcholine in muscle tissue is only attributable to the motorneuron terminals. This result, together with the similarity between genotypes in the staining of the acetylcholine receptors at the endplates, suggests that cholinergic neurotransmission is not affected in muscle from KI males, at least in young animals. However, whether there are other alterations in motorneurons despite the similar neurotransmitter levels and/or whether the aging process affects differentially these cells and tissues with high energy demand in the brain and muscle Cr deficient KI rats is not known and further investigations would be needed.

On the other hand, free choline in muscle tissue is present not only in motorneurons but in other cells such as myocytes. Choline is also the precursor of choline phospholipids, important for cellular membranes, and S-adenosyl-methionine, important in the methylation of molecules such as GAA for the synthesis of Cr. Such significant increase in choline concentration could affect the pool of all or

some of the mentioned products and correlated with the increase in GAA concentration, suggesting that these changes might be related with the possible attempt in increasing Cr levels in muscle from KI males.

In summary, we characterized the motor function phenotype of the *Slc6a8*$^{xY389C/y}$ KI rat males and provided more cues about the pathology of CTD and the *in vivo* effects of Cr deficiency in muscle and in cerebellum.

Table 3: Comparisons of different features among rat and mouse models of CTD and CTD patients.

↓, significant decreased; ↑, significant increased; low, decreased but in normal range; n.s., no significant differences; NA, not analyzed; YES, feature present; YES*, feature clearly present in one [33] and mentioned but not fully demonstrated in other [11]; NO, feature absent; a, (Stockebrand et al., 2018); b, (Baroncelli et al., 2014); c, (Baroncelli et al., 2016); d, (Skelton et al., 2011); e (Wawro et al., 2021); f (Duran-Trio et al., 2021); g (Pyne-Geithman et al., 2004); h (van de Kamp et al., 2014).

	Mice	**Rat**	**Patient(s)**
Muscle mass	↓ [a]	↓	↓
Muscle Cr concentration	↓ [abcd]	↓	n.s. (*n*=1)
Muscle GAA concentration	↑ [c]	↑	NA
Myocyte size	↓ [ae]	↓	NA
atrophy	YES* [ae]	NO	NO (*n*=1 [g])
Plasmatic CK	NA	low	↓(*n*=1) / n.s. (*n*=1) [h]
Plasmatic Cr concentration	↓ [d]	↓ [f]	n.s. [h]
Plasmatic GAA concentration	NA	↑ [f]	n.s. [h]
Motor dysfunction	YES [a]	YES	YES [h]
Cerebellar alterations	NA	YES	YES [h]

ACKNOWLEDGEMENTS

This work was supported by the Swiss National Science Foundation (Grant n° 31003A-175778). We thank Marc Loup, Marc Lanzillo, Dario Sessa, Ana Versace and Annie-Juliette Ferrari-Gyger for excellent technical help. The authors declare no competing financial interests.

AUTHOR CONTRIBUTIONS:

LDT and OB designed the study and wrote the manuscript; LDT and GFP handled the animals and collected samples and liquids; CR and PAB performed Cr, GAA, Crn and CK measures; LDT performed acetylcholine and choline measures; LDT, JG and CS designed and performed the behavioral tests; experiments and analysis of gene expression and western blots were designed and performed by ISA and KDB; fluorescence and histological studies were performed by LDT; Golgi-Cox staining was performed by GFP and LDT and dendritic spine studies by LDT; LDT analyzed the data; all resources needed to perform this work were provided by OB, CC, CS and KDB; OB and CC secured the financial support of this work; all authors reviewed and corrected the manuscript.

Bibliography:

1 Sestili, P., Martinelli, C., Colombo, E., Barbieri, E., Potenza, L., Sartini, S. & Fimognari, C. Creatine as an antioxidant. *Amino Acids* **40**, 1385-1396, doi:10.1007/s00726-011-0875-5 (2011).

2 Hanna-El-Daher, L. & Braissant, O. Creatine synthesis and exchanges between brain cells: what can be learned from human creatine deficiencies and various experimental models? *Amino acids* **48**, 1877-1895 (2016).

3 Wyss, M. & Kaddurah-Daouk, R. Creatine and creatinine metabolism. *Physiol Rev* **80**, 1107-1213, doi:10.1152/physrev.2000.80.3.1107 (2000).

4 Item, C. B., Stockler-Ipsiroglu, S., Stromberger, C., Muhl, A., Alessandri, M. G., Bianchi, M. C., Tosetti, M., Fornai, F. & Cioni, G. Arginine:glycine amidinotransferase deficiency: the third inborn error of creatine metabolism in humans. *Am J Hum Genet* **69**, 1127-1133, doi:10.1086/323765 (2001).

5 Schulze, A. & Braissant, O. in *Pediatric Endocrinology and Inborn Errors of Metabolism* (eds K. Sarafoglou, Hoffmann, G. F. & & K. S. Roth) Ch. Creatine Deficiency Syndromes, 181–190 (McGraw Hill, 2017).

6 Salomons, G. S., van Dooren, S. J., Verhoeven, N. M., Cecil, K. M., Ball, W. S., Degrauw, T. J. & Jakobs, C. X-linked creatine-transporter gene (SLC6A8) defect: a new creatine-deficiency syndrome. *Am J Hum Gen* **68**, 1497-1500, doi:10.1086/320595 (2001).

7 Stockler, S., Holzbach, U., Hanefeld, F., Marquardt, I., Helms, G., Requart, M., Hanicke, W. & Frahm, J. Creatine deficiency in the brain: a new, treatable inborn error of metabolism. *Pediatr Res* **36**, 409-413, doi:10.1203/00006450-199409000-00023 (1994).

8 van de Kamp, J. M., Mancini, G. M. & Salomons, G. S. X-linked creatine transporter deficiency: clinical aspects and pathophysiology. *J Inherit Metab Dis* **37**, 715-733, doi:10.1007/s10545-014-9713-8 (2014).

9 Skelton, M. R., Schaefer, T. L., Graham, D. L., Degrauw, T. J., Clark, J. F., Williams, M. T. & Vorhees, C. V. Creatine transporter (CrT; Slc6a8) knockout mice as a model of human CrT deficiency. *PloS One* **6**, e16187, doi:10.1371/journal.pone.0016187 (2011).

10 Baroncelli, L., Alessandri, M. G., Tola, J., Putignano, E., Migliore, M., Amendola, E., Gross, C., Leuzzi, V., Cioni, G. & Pizzorusso, T. A novel mouse model of creatine transporter deficiency. *F1000Research* **3**, 228, doi:10.12688/f1000research.5369.1 (2014).

11 Stockebrand, M., Sasani, A., Das, D., Hornig, S., Hermans-Borgmeyer, I., Lake, H. A., Isbrandt, D., Lygate, C. A., Heerschap, A., Neu, A. & Choe, C. U. A Mouse Model of Creatine

Transporter Deficiency Reveals Impaired Motor Function and Muscle Energy Metabolism. *Front Physiol* **9**, 773, doi:10.3389/fphys.2018.00773 (2018).

12 Duran-Trio, L., Fernandes-Pires, G., Simicic, D., Grosse, J., Roux-Petronelli, C., Bruce, S. J., Binz, P. A., Sandi, C., Cudalbu, C. & Braissant, O. A new rat model of creatine transporter deficiency reveals behavioral disorder and altered brain metabolism. *Sci Rep* **11**, 1636, doi:10.1038/s41598-020-80824-x (2021).

13 Udobi, K. C., Delcimmuto, N., Kokenge, A. N., Abdulla, Z. I., Perna, M. K. & Skelton, M. R. Deletion of the creatine transporter gene in neonatal, but not adult, mice leads to cognitive deficits. *J Inherit Metab Dis* **42**, 966-974 (2019).

14 Baroncelli, L., Molinaro, A., Cacciante, F., Alessandri, M. G., Napoli, D., Putignano, E., Tola, J., Leuzzi, V., Cioni, G. & Pizzorusso, T. A mouse model for creatine transporter deficiency reveals early onset cognitive impairment and neuropathology associated with brain aging. *Hum Mol Gen* **25**, 4186-4200, doi:10.1093/hmg/ddw252 (2016).

15 Molinaro, A., Alessandri, M. G., Putignano, E., Leuzzi, V., Cioni, G., Baroncelli, L. & Pizzorusso, T. A Nervous System-Specific Model of Creatine Transporter Deficiency Recapitulates the Cognitive Endophenotype of the Disease: a Longitudinal Study. *Sci Rep* **9**, 62, doi:10.1038/s41598-018-37303-1 (2019).

16 Abdulla, Z. I., Pennington, J. L., Gutierrez, A. & Skelton, M. R. Creatine transporter knockout mice (Slc6a8) show increases in serotonin-related proteins and are resilient to learned helplessness. *Behav Brain Res* **377**, 112254 (2020).

17 Kurosawa, Y., Degrauw, T. J., Lindquist, D. M., Blanco, V. M., Pyne-Geithman, G. J., Daikoku, T., Chambers, J. B., Benoit, S. C. & Clark, J. F. Cyclocreatine treatment improves cognition in mice with creatine transporter deficiency. *J Clin Invest* **122**, 2837-2846, doi:10.1172/JCI59373 (2012).

18 Udobi, K. C., Kokenge, A. N., Hautman, E. R., Ullio, G., Coene, J., Williams, M. T., Vorhees, C. V., Mabondzo, A. & Skelton, M. R. Cognitive deficits and increases in creatine precursors in a brain-specific knockout of the creatine transporter gene Slc6a8. *Genes Brain Behav* **17**, e12461, doi:10.1111/gbb.12461 (2018).

19 Perna, M. K., Kokenge, A. N., Miles, K. N., Udobi, K. C., Clark, J. F., Pyne-Geithman, G. J., Khuchua, Z. & Skelton, M. R. Creatine transporter deficiency leads to increased whole body and cellular metabolism. *Amino Acids* **48**, 2057-2065, doi:10.1007/s00726-016-2291-3 (2016).

20 Mazziotti, R., Cacciante, F., Sagona, G., Lupori, L., Gennaro, M., Putignano, E., Alessandri, M. G., Ferrari, A., Battini, R., Cioni, G., Pizzorusso, T. & Baroncelli, L. Novel translational phenotypes and biomarkers for creatine transporter deficiency. *Brain Commun* **2**, fcaa089, doi:10.1093/braincomms/fcaa089 (2020).

21 Sartini, S., Lattanzi, D., Ambrogini, P., Di Palma, M., Galati, C., Savelli, D., Polidori, E., Calcabrini, C., Rocchi, M. B., Sestili, P. & Cuppini, R. Maternal creatine supplementation affects the morpho-functional development of hippocampal neurons in rat offspring. *Neuroscience* **312**, 120-129, doi:10.1016/j.neuroscience.2015.11.017 (2016).

22 Braissant, O., Henry, H., Villard, A.-M., Zurich, M.-G., Loup, M., Eilers, B., Parlascino, G., Matter, E., Boulat, O. & Honegger, P. Ammonium-induced impairment of axonal growth is prevented through glial creatine. *J Neurosci* **22**, 9810-9820, doi:10.1523/JNEUROSCI.22-22-09810.2002 (2002).

23 Ducray, A. D., Schlappi, J. A., Qualls, R., Andres, R. H., Seiler, R. W., Schlattner, U., Wallimann, T. & Widmer, H. R. Creatine treatment promotes differentiation of GABA-ergic neuronal precursors in cultured fetal rat spinal cord. *J Neurosci Res* **85**, 1863-1875, doi:10.1002/jnr.21337 (2007).

24 Sestili, P., Ambrogini, P., Barbieri, E., Sartini, S., Fimognari, C., Calcabrini, C., Diaz, A. R., Guescini, M., Polidori, E., Luchetti, F., Canonico, B., Lattanzi, D., Cuppini, R., Papa, S. & Stocchi, V. New insights into the trophic and cytoprotective effects of creatine in in vitro and in vivo models of cell maturation. *Amino Acids* **48**, 1897-1911, doi:10.1007/s00726-015-2161-4 (2016).

25 Pyne-Geithman, G. J., deGrauw, T. J., Cecil, K. M., Chuck, G., Lyons, M. A., Ishida, Y. & Clark, J. F. Presence of normal creatine in the muscle of a patient with a mutation in the creatine

transporter: a case study. *Mol Cell Biochem* **262**, 35-39, doi:10.1023/b:mcbi.0000038213.15646.4a (2004).

26 Ellenbroek, B. & Youn, J. Rodent models in neuroscience research: is it a rat race? *Dis Models Mech* **9**, 1079-1087 (2016).

27 Braissant, O., Cagnon, L., Monnet-Tschudi, F., Speer, O., Wallimann, T., Honegger, P. & Henry, H. Ammonium alters creatine transport and synthesis in a 3D culture of developing brain cells, resulting in secondary cerebral creatine deficiency. *Eur J Neurosci* **27**, 1673-1685, doi:10.1111/j.1460-9568.2008.06126.x (2008).

28 Team, R. C. R: A Language and Environment for Statistical Computing (Version 3.5. 1, R Foundation for Statistical Computing, Vienna, Austria, 2018). *https://www.R-project.org/*. (2018).

29 Bates, D., Mächler, M., Bolker, B. & Walker, S. Fitting Linear Mixed-Effects Models Usinglme4. *J Stat Soft* **67**, 1-48, doi:10.18637/jss.v067.i01 (2015).

30 Wickham, H. *ggplot2: elegant graphics for data analysis*. (Springer, 2016).

31 Kashani, K., Rosner, M. H. & Ostermann, M. Creatinine: From physiology to clinical application. *Eur J Intern Med* **72**, 9-14, doi:10.1016/j.ejim.2019.10.025 (2020).

32 Mukund, K. & Subramaniam, S. Skeletal muscle: A review of molecular structure and function, in health and disease. *Wiley Interdiscip Rev Syst Biol Med* **12**, e1462, doi:10.1002/wsbm.1462 (2020).

33 Wawro, A. M., Gajera, C. R., Baker, S. A., Nirschl, J. J., Vogel, H. & Montine, T. J. Creatine transport and pathological changes in creatine transporter deficient mice. *J Inherit Metab Dis* **44**, 939-948, doi:10.1002/jimd.12358 (2021).

34 Sandri, M., Sandri, C., Gilbert, A., Skurk, C., Calabria, E., Picard, A., Walsh, K., Schiaffino, S., Lecker, S. H. & Goldberg, A. L. Foxo transcription factors induce the atrophy-related ubiquitin ligase atrogin-1 and cause skeletal muscle atrophy. *Cell* **117**, 399-412, doi:10.1016/s0092-8674(04)00400-3 (2004).

35 Lallemand, F., Seo, S. R., Ferrand, N., Pessah, M., L'Hoste, S., Rawadi, G., Roman-Roman, S., Camonis, J. & Atfi, A. AIP4 restricts transforming growth factor-β signaling through a ubiquitination-independent mechanism. *J Biol Chem* **280**, 27645-27653 (2005).

36 Le Grand, J. N., Chakrama, F. Z., Seguin-Py, S., Fraichard, A., Delage-Mourroux, R., Jouvenot, M. & Boyer-Guittaut, M. GABARAPL1 (GEC1): original or copycat? *Autophagy* **7**, 1098-1107, doi:10.4161/auto.7.10.15904 (2011).

37 Britto, F. A., Dumas, K., Giorgetti-Peraldi, S., Ollendorff, V. & Favier, F. B. Is REDD1 a metabolic double agent? Lessons from physiology and pathology. *Am J Physiol Cell Physiol* **319**, C807-C824, doi:10.1152/ajpcell.00340.2020 (2020).

38 Meyuhas, O. Ribosomal Protein S6 Phosphorylation: Four Decades of Research. *Int Rev Cell Mol Biol* **320**, 41-73, doi:10.1016/bs.ircmb.2015.07.006 (2015).

39 Valdez, G., Tapia, J. C., Kang, H., Clemenson, G. D., Jr., Gage, F. H., Lichtman, J. W. & Sanes, J. R. Attenuation of age-related changes in mouse neuromuscular synapses by caloric restriction and exercise. *Proc Natl Acad Sci U S A* **107**, 14863-14868, doi:10.1073/pnas.1002220107 (2010).

40 van de Kamp, J. M., Betsalel, O. T., Mercimek-Mahmutoglu, S., Abulhoul, L., Grunewald, S., Anselm, I., Azzouz, H., Bratkovic, D., de Brouwer, A., Hamel, B., Kleefstra, T., Yntema, H., Campistol, J., Vilaseca, M. A., Cheillan, D., D'Hooghe, M., Diogo, L., Garcia, P., Valongo, C., Fonseca, M., Frints, S., Wilcken, B., von der Haar, S., Meijers-Heijboer, H. E., Hofstede, F., Johnson, D., Kant, S. G., Lion-Francois, L., Pitelet, G., Longo, N., Maat-Kievit, J. A., Monteiro, J. P., Munnich, A., Muntau, A. C., Nassogne, M. C., Osaka, H., Ounap, K., Pinard, J. M., Quijano-Roy, S., Poggenburg, I., Poplawski, N., Abdul-Rahman, O., Ribes, A., Arias, A., Yaplito-Lee, J., Schulze, A., Schwartz, C. E., Schwenger, S., Soares, G., Sznajer, Y., Valayannopoulos, V., Van Esch, H., Waltz, S., Wamelink, M. M., Pouwels, P. J., Errami, A., van der Knaap, M. S., Jakobs, C., Mancini, G. M. & Salomons, G. S. Phenotype and genotype in 101 males with X-linked creatine transporter deficiency. *J Med Genet* **50**, 463-472, doi:10.1136/jmedgenet-2013-101658 (2013).

41 Dehmelt, L. & Halpain, S. The MAP2/Tau family of microtubule-associated proteins. *Genome Biol* **6**, 204, doi:10.1186/gb-2004-6-1-204 (2005).

42 Yuan, A., Rao, M. V., Veeranna & Nixon, R. A. Neurofilaments and Neurofilament Proteins in Health and Disease. *Cold Spring Harb Perspect Biol* **9**, doi:10.1101/cshperspect.a018309 (2017).

43 Assentoft, M., Larsen, B. R. & MacAulay, N. Regulation and Function of AQP4 in the Central Nervous System. *Neurochem Res* **40**, 2615-2627, doi:10.1007/s11064-015-1519-z (2015).

44 Takahashi, M. & Shinoda, Y. Neural Circuits of Inputs and Outputs of the Cerebellar Cortex and Nuclei. *Neuroscience* **462**, 70-88, doi:10.1016/j.neuroscience.2020.07.051 (2021).

45 Nimchinsky, E. A., Sabatini, B. L. & Svoboda, K. Structure and function of dendritic spines. *Annu Rev Physiol* **64**, 313-353, doi:10.1146/annurev.physiol.64.081501.160008 (2002).

46 Cruz, P. M. R., Cossins, J., Beeson, D. & Vincent, A. The neuromuscular junction in health and disease: molecular mechanisms governing synaptic formation and homeostasis. *Front Mol Neurosci* **13** (2020).

47 Banfi, G., Colombini, A., Lombardi, G. & Lubkowska, A. Metabolic markers in sports medicine. *Adv Clin Chem* **56**, 1-54, doi:10.1016/b978-0-12-394317-0.00015-7 (2012).

48 Kaviani, M., Shaw, K. & Chilibeck, P. D. Benefits of Creatine Supplementation for Vegetarians Compared to Omnivorous Athletes: A Systematic Review. *Int J Environ Res Public Health* **17**, 3041, doi:10.3390/ijerph17093041 (2020).

49 Torremans, A., Marescau, B., Possemiers, I., Van Dam, D., D'Hooge, R., Isbrandt, D. & De Deyn, P. P. Biochemical and behavioural phenotyping of a mouse model for GAMT deficiency. *J Neurol Sci* **231**, 49-55, doi:10.1016/j.jns.2004.12.014 (2005).

50 Choe, C. U., Nabuurs, C., Stockebrand, M. C., Neu, A., Nunes, P., Morellini, F., Sauter, K., Schillemeit, S., Hermans-Borgmeyer, I., Marescau, B., Heerschap, A. & Isbrandt, D. L-arginine:glycine amidinotransferase deficiency protects from metabolic syndrome. *Hum Mol Genet* **22**, 110-123, doi:10.1093/hmg/dds407 (2013).

51 Brault, J. J., Abraham, K. A. & Terjung, R. L. Muscle creatine uptake and creatine transporter expression in response to creatine supplementation and depletion. *J Appl Physiol (1985)* **94**, 2173-2180, doi:10.1152/japplphysiol.01171.2002 (2003).

52 Russell, A. P., Ghobrial, L., Wright, C. R., Lamon, S., Brown, E. L., Kon, M., Skelton, M. R. & Snow, R. J. Creatine transporter (SLC6A8) knockout mice display an increased capacity for in vitro creatine biosynthesis in skeletal muscle. *Front Physiol* **5**, 314, doi:10.3389/fphys.2014.00314 (2014).

53 Guthmiller, P., Van Pilsum, J. F., Boen, J. R. & McGuire, D. M. Cloning and sequencing of rat kidney L-arginine:glycine amidinotransferase. Studies on the mechanism of regulation by growth hormone and creatine. *J Biol Chem* **269**, 17556-17560 (1994).

54 Wax, B., Kerksick, C. M., Jagim, A. R., Mayo, J. J., Lyons, B. C. & Kreider, R. B. Creatine for Exercise and Sports Performance, with Recovery Considerations for Healthy Populations. *Nutrients* **13**, 1915, doi:10.3390/nu13061915 (2021).

55 Braissant, O., Henry, H., Loup, M., Eilers, B. & Bachmann, C. Endogenous synthesis and transport of creatine in the rat brain: an in situ hybridization study. *Brain Res Mol Brain Res* **86**, 193-201, doi:10.1016/s0169-328x(00)00269-2 (2001).

56 Xu, H., Yang, Y., Tang, X., Zhao, M., Liang, F., Xu, P., Hou, B., Xing, Y., Bao, X. & Fan, X. Bergmann glia function in granule cell migration during cerebellum development. *Mol Neurobiol* **47**, 833-844, doi:10.1007/s12035-013-8405-y (2013).

57 Bellamy, T. C. Interactions between Purkinje neurones and Bergmann glia. *The Cerebellum* **5**, 116-126 (2006).

58 Allen, N. J. & Lyons, D. A. Glia as architects of central nervous system formation and function. *Science* **362**, 181-185, doi:10.1126/science.aat0473 (2018).

59 Berry, K. P. & Nedivi, E. Spine Dynamics: Are They All the Same? *Neuron* **96**, 43-55, doi:10.1016/j.neuron.2017.08.008 (2017).

SUPPLEMENTARY MATERIAL

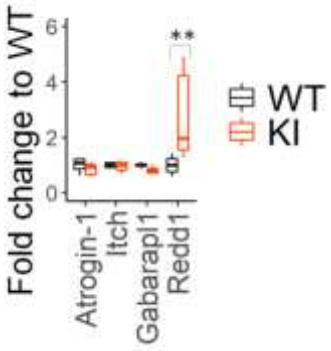

Supplementary Figure 1: Muscle expression levels (by quantitative PCR) of Atrogin-1, Itch, Gabarapl1 and Redd1 from WT and KI males (black and orange boxes, respectively). GAPDH was used as housekeeping gene for normalization. 4 WT and 5 KI; 2-way ANOVA and Tukey posthoc test. ***P*<0.01, ****P*<0.001. Statistical analysis was conducted with R-3.5.1 [28]. Graphs were done using ggplot2 package [30].

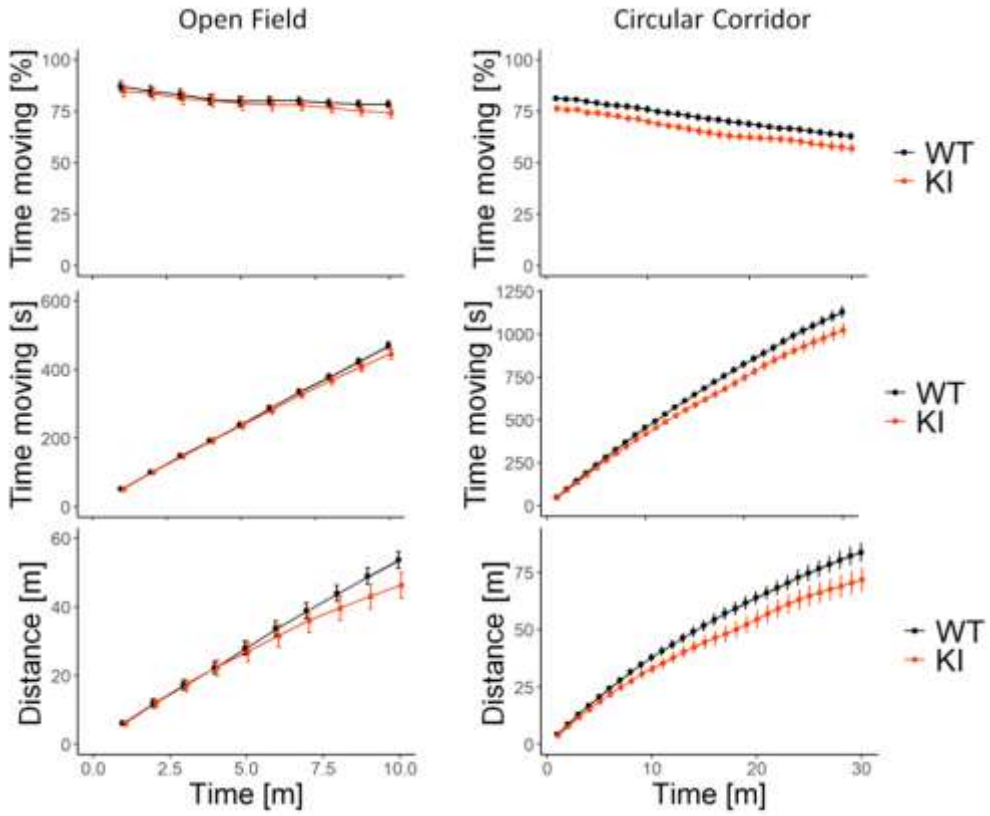

Supplementary Figure 2: Cumulative time moving and cumulative distance along time in open field and circular corridor tests.

No differences were found between genotypes in the open field test in cumulative time moving (in % and in seconds, upper and middle left panels respectively) or cumulative distance moved (in meters, bottom left panel) at any time. 10 WT and 10 KI males.

In circular corridor test, KI males spent significantly (*P*<0.05) less time moving from the first minute (upper and middle right panels) and moved significantly less distance from minute 7 (bottom right panel) in comparison with WT males. 9 WT and 10 KI males.

Linear mixed models blocking litter as random factor. Statistical analysis was conducted with R-3.5.1 [28], package lme4 [29]. Graphs were done using ggplot2 package [30].